Chapter 9
Stable Isotope Signatures of Authigenic Minerals from Methane Seeps

Shanggui Gong, Jörn Peckmann, and Dong Feng

Abstract Authigenic minerals forming at marine seeps constitute an excellent archive of past methane seepage and biogeochemical processes. Over the past two decades, authigenic carbonate and sulfur-bearing minerals from methane seeps of the South China Sea (SCS) have been widely investigated, providing insight into fluid sources and seepage dynamics and facilitating the establishment of geochemical proxies to trace sulfate-driven anaerobic oxidation of methane (SD-AOM). Authigenic carbonates from all seep sites in the SCS commonly exhibit low $\delta^{13}C$ and high $\delta^{18}O$ values, confirming the incorporation of methane-derived carbon and oxygen from a pore water pool probably affected by gas hydrate dissociation. Pyrite is a common authigenic mineral at methane seeps, also forming at low methane flux where authigenic carbonate tends to be absent. The identification of methane seepage and SD-AOM activity consequently benefited from the advancement of sulfur isotope geochemistry, particularly from in situ measurements of $\delta^{34}S_{pyrite}$ values using nanoSIMS and multiple sulfur isotopes. Quantification of carbon and sulfur fluxes in the course of SD-AOM in modern and ancient marine sedimentary environments remains challenging, highlighting the need for more field-based research and modeling work. Furthermore, other elemental cycles and biogeochemical processes at methane seeps archived in authigenic minerals, such as nitrogen-based metabolisms, remain largely unknown. We highlight that SCS seeps are fascinating natural laboratories to better understand methane-driven biogeochemical processes and their signatures in authigenic minerals, representing a rewarding but also challenging object of research in the field of geomicrobiology.

S. Gong (✉) · D. Feng
College of Marine Sciences, Shanghai Ocean University, Shanghai 201306, China
e-mail: sggong@shou.edu.cn

D. Feng
e-mail: dfeng@shou.edu.cn

J. Peckmann
Institute for Geology, Center for Earth System Research and Sustainability, Universität Hamburg, 20146 Hamburg, Germany
e-mail: joern.peckmann@uni-hamburg.de

D. Chen and D. Feng (eds.), *South China Sea Seeps*,
https://doi.org/10.1007/978-981-99-1494-4_9

9.1 Introduction

Authigenic minerals resulting from sulfate-driven anaerobic methane oxidation (SD-AOM) constitute a unique archive of past methane seepage and biogeochemical processes. As the key process at marine seeps, SD-AOM represents the main methane sink in marine sedimentary environments (Boetius et al. 2000; Reeburgh 2007; Egger et al. 2018), providing the local chemotrophic community with energy (Campbell 2006; Suess et al. 2018; Yang et al. 2020), regulating greenhouse gas emissions at the seafloor (Olson et al. 2016), and representing a hotspot of the marine carbon and sulfur cycles (Peckmann and Thiel 2004; Hu et al. 2022). SD-AOM releases dissolved bicarbonate and hydrogen sulfide, thereby favoring the precipitation of authigenic carbonate and sulfide minerals in the shallow sedimentary subsurface at marine seeps (Boetius et al. 2000). In turn, authigenic carbonate and sulfide and other sulfur-bearing minerals archive locally prominent biogeochemical process in the form of diagnostic stable isotope, trace element, and lipid biomarker patterns (Peckmann and Thiel 2004; Feng et al. 2016; Smrzka et al. 2019, 2020; Lin et al. 2022). These authigenic minerals record modes of methane transport and early diagenetic environments and allow the exploration of the role of methane in Earth's surface environments by tracing SD-AOM activity (Peckmann and Thiel 2004; Feng et al. 2016, 2018; Gong et al. 2022).

Authigenic carbonates with different mineralogies and carbon and oxygen isotope compositions have been widely reported from the South China Sea (SCS; Chen et al. 2005; Han et al. 2008, 2014; Tong et al. 2013; Wang et al. 2014; Feng and Chen 2015; Liang et al. 2017; Huang et al. 2022b). The morphologies of these seep carbonates vary, including crusts, mounds, pipes, tubes, and highly irregular bodies, reflecting different seepage intensities and the interaction of burrowing megafauna with fluid migration (Fig. 9.1; Han et al. 2013; Feng and Chen 2015; Sun et al. 2020b; Lu et al. 2021). Multiple carbonate mineral phases have been identified in the SCS, including aragonite, low-Mg calcite, high-Mg calcite, and dolomite (Fig. 9.2). These carbonates mainly consist of microcrystalline minerals, particularly calcite and dolomite (Fig. 9.3), with larger cement crystals typically represented by aragonite (Feng and Chen 2015). The formation of carbonate is governed by supersaturation, dissolved species concentration (Ca^{2+} and Mg^{2+}, SO_4^{2-}, and PO_4^{3-}), and microbial activity, all of which are highly variable in space and time due to changing methane flux (Peckmann et al. 2001; Luff and Wallmann 2003; Feng and Chen 2015; Gong et al. 2018a; Tong et al. 2019; Lu et al. 2021). In general, the occurrence of aragonite reflects a relatively high methane flux, where high levels of carbonate supersaturation and sulfate concentration as well as relatively low levels of sulfide favor aragonite over calcite precipitation (Burton 1993; Luff and Wallmann 2003). Combined with mineralogical analysis, trace element and lipid biomarker inventories allow to constrain the dynamics of the seep activity by reconstructing redox conditions (Feng and Chen 2015; Guan et al. 2016; Liang et al. 2017, 2022; Gong et al. 2018a; Smrzka et al. 2020). The carbon and oxygen isotope compositions of authigenic carbonates are established proxies to reconstruct the composition and temperature of fluids from

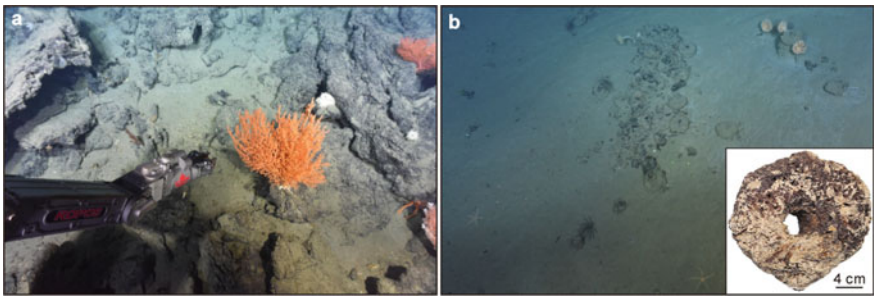

Fig. 9.1 Seafloor images of typical seep manifestations. **a** Massive carbonate crusts; **b** tubular carbonate exposed on the seafloor. Image collected at the Jiulong methane reef (water depth: 684 m) during *ROPOS* dives 2070 and 2073 in 2018

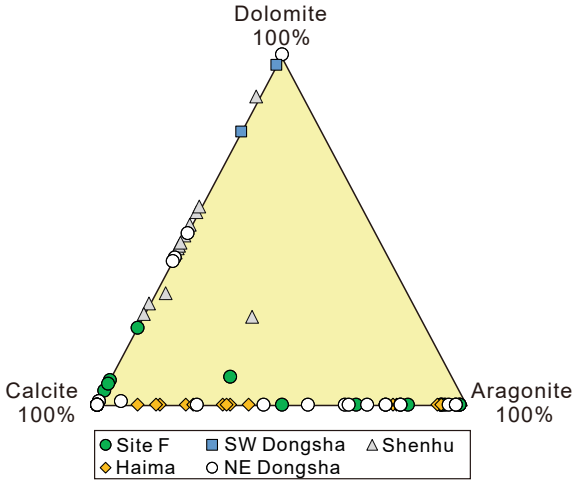

Fig. 9.2 Composition of the carbonate fraction in seep carbonates at South China Sea. Data are from Tong et al. (2013), Han et al. (2014), Feng and Chen (2015), Lu et al. (2015) and Liang et al. (2017)

which carbonates precipitated, promoting the understanding of the sources and potential forces of methane seepage in the South China Sea (Chen et al. 2005; Han et al. 2008, 2013; Feng et al. 2015; Liang et al. 2017; Feng et al. 2018).

The extremely negative $\delta^{13}C$ values of authigenic seep carbonates are recognized as the most distinctive geological feature of SD-AOM inherited from the ^{13}C depletion of biogenic methane (−110‰ to −50‰) and thermogenic methane (−50‰ to −30‰; Sackett 1978; Whiticar 1999; Peckmann et al. 2001; Chen et al. 2005). The $\delta^{13}C_{carbonate}$ signature of SD-AOM can be masked by admixture of dissolved inorganic carbon (DIC) from sources other than methane oxidation: DIC sourced from organoclastic sulfate reduction (OSR), seawater DIC with a $\delta^{13}C$ value of 0‰, and a residual ^{13}C-enriched pool after methanogenesis (Feng et al. 2018). Admixture of DIC from other sources than methane oxidation was probably more common in paleooceans before the early Paleozoic Era, which were characterized by high seawater

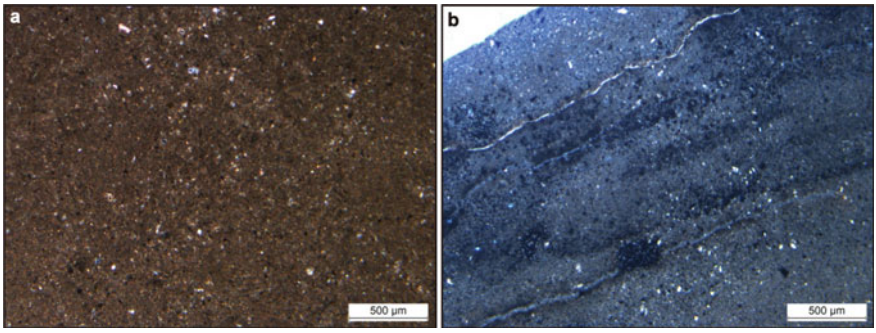

Fig. 9.3 Thin section photomicrographs of seep carbonate obtained from Site F, plane-polarized light (details in Feng and Chen 2015). **a** Typical microcrystalline carbonate matrix with enclosed terrigenous sediment. **b** Microcrystalline carbonate with abundant pyrite framboids (dark) enclosed

DIC and/or low seawater sulfate levels resulting in a lower ratio of SD-AOM-sourced DIC and seawater DIC (Bristow and Grotzinger 2013). Furthermore, the $\delta^{13}C$ proxy typically cannot be employed for tracing SD-AOM in methane diffusion-limited settings, as authigenic carbonate tends to form only in settings with relatively high methane flux (Luff and Wallmann 2003; Hu et al. 2020).

Fortunately, sulfur-bearing minerals, benefiting from recent advances in sulfur isotope biogeochemistry, can be used to identify SD-AOM even in low flux settings and to constrain the sulfur cycle in methane-bearing environments (Jørgensen et al. 2004; Chen et al. 2006; Feng and Robert 2011; Lin et al. 2015, 2016a, b, 2017; Li et al. 2016; Gong et al. 2018a, b; Liu et al. 2022a). Innovative approaches have been applied and new understanding has been obtained thanks to research on seepage in the SCS: (1) environmental controls on the morphology and $\delta^{34}S$ of SD-AOM-derived pyrite (Chen et al. 2005; Lin et al. 2016a, b, 2017; Li et al. 2016; Gong et al. 2018a); (2) the extremely high variability of $\delta^{34}S$ in SD-AOM-derived pyrite via nanoSIMS analysis (Lin et al. 2016a, b); (3) a carbonate-based proxy for SD-AOM (Feng et al. 2016); and (4) diagnostic multiple sulfur isotope systematics of SD-AOM (Lin et al. 2017; Gong et al. 2018b, 2022; Liu et al. 2020, 2022a). These achievements provide a robust approach for SD-AOM tracing in the subrecent marine sedimentary record and the older rock record and promise deeper future insight into the mechanisms of pyritization during early diagenesis, which are key requirements for reconstructing the global sulfur cycle (Wang et al. 2021; Peng et al. 2022).

Overall, methane-derived authigenic carbonate and sulfide minerals provide a useful geological archive of fluid composition, past SD-AOM activity, and early diagenetic environments. In this chapter, we review the current knowledge of the key biogeochemical processes archived in methane-derived authigenic carbonate and sulfide minerals from a stable carbon, oxygen, and sulfur isotope geochemistry perspective, focusing on (1) the recognition of biogeochemical processes and fluid sources archived in authigenic carbonates and (2) the sulfur isotope systematics of SD-AOM in modern marine sediments and its implication for tracing past SD-AOM.

9.2 Fluid Sources and Biogeochemical Processes Archived in Authigenic Carbonate Minerals

9.2.1 C–O Isotope Signatures of Methane-Derived Authigenic Carbonate

^{13}C-depleted carbonates found at all seep sites of the SCS revealed that precipitation was predominantly driven by microbial oxidation of methane (Fig. 9.4; Chen et al. 2005; Han et al. 2008, 2013, 2014; Tong et al. 2013; Wang et al. 2014; Feng and Chen 2015; Liang et al. 2017; Lu et al. 2017; Yang et al. 2018). Biological methane sources have been identified across seep sites in the SCS based on the δ^{13}C values of methane and DIC (Chuang et al. 2013; Zhuang et al. 2016; Hu et al. 2018, 2019; Jin et al. 2022). However, the δ^{13}C values of carbonates in the SCS are typically higher than −50‰, indicating significant admixture of DIC from other sources than methane oxidation, including seawater, decomposition of organic matter, and residual DIC after methanogenesis (Peckmann and Thiel 2004; Feng et al. 2018; Huang et al. 2022a). The great variability of δ^{13}C values indicates that the degree of mixing among the different DIC pools varies in both space and time. Therefore, the δ^{13}C values of lipid biomarkers are better proxies to identify different methane sources (Himmler et al. 2015; Guan et al. 2016, 2018). Furthermore, high resolution measurement δ^{13}C values of carbonate with nanoSIMS analysis is another promising tool to determine methane sources (Feng et al. 2018).

The oxygen isotope composition of authigenic carbonates provides the means to calculate the temperature during precipitation and the δ^{18}O value of the parent fluid (Naehr et al. 2007; Han et al. 2014). The δ^{18}O value of authigenic carbonate is controlled by a combination of factors, including (1) mineralogy and chemistry, (2) ambient temperature, and (3) δ^{18}O value of the parent fluid (Anderson and Arthur 1983; Grossman and Ku 1986; Kim and O'Neil 1997; Mavromatis et al. 2012). Many seep carbonates collected from the SCS exhibit δ^{18}O values higher than the calculated equilibrium values based on the mineral type, bottom water temperature, and δ^{18}O value of seawater (Feng and Chen 2015; Liang et al. 2017; Yang et al. 2018). This ^{18}O enrichment can be explained by the addition of ^{18}O-rich fluids resulting from gas hydrate dissociation (Bohrmann et al. 1998; Han et al. 2013; Feng and Chen 2015; Liang et al. 2017). However, ^{18}O-rich fluids could also originate from clay mineral dehydration (Hesse 2003) and deep-sourced fluids modified by mineral–water interactions (Holser et al. 1979; Giggenbach 1992). Therefore, the sources of ^{18}O-rich fluids and their diagnostic signatures require further study. Reconstruction of the temperature during carbonate precipitation can provide additional information on the environmental settings at methane seeps. However, due to the variable δ^{18}O values of parent fluids, the paleo-temperature during carbonate precipitation cannot be calculated using δ^{18}O values alone. Recently, a carbonate clumped isotope (Δ_{47}) thermometer has been explored for methane-derived authigenic carbonates (Wacker

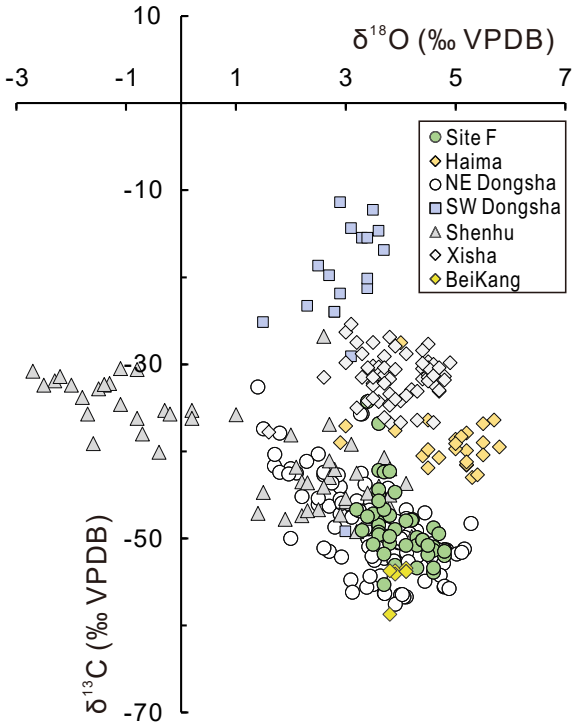

Fig. 9.4 Compilation of published $\delta^{13}C$ and $\delta^{18}O$ values of seep carbonates retrieved from the South China Sea. Data are from Chen et al. (2005); Han et al. (2008, 2014); Tong et al. (2013); Feng and Chen (2015); Lu et al. (2015, 2018); Liang et al. (2017); Huang et al. (2022a) and Liu et al. (2022b)

et al. 2014; Loyd et al. 2016; Zhang et al. 2019; Thiagarajan et al. 2020). Both equilibrium and disequilibrium clumped isotope values have been reported for methane-derived authigenic carbonates, highlighting that additional proxies (e.g., Δ_{48}) are needed to further constrain the factors (e.g., the kinetic isotope effect) affecting the Δ_{47} value, hopefully allowing for more accurate paleotemperature reconstructions in the future.

9.2.2 Diagnostic $\delta^{18}O_{SO4}$ Versus $\delta^{34}S_{SO4}$ Patterns of SD-AOM

Since the signature of ^{13}C depletion of SD-AOM can be diluted by admixture of DIC from other sources than methane oxidation, a new carbonate-based proxy for SD-AOM has been established by Feng et al. (2016). The work of these authors emphasized that the isotopic signal of porewater sulfate can be preserved in authigenic carbonate in the form of carbonate-associated sulfate. For a given porewater sulfate profile, the slope of the tangent along the gradient of $\delta^{18}O_{SO4}$ and $\delta^{34}S_{SO4}$ values (referred to as the $\delta^{18}O_{SO4}/\delta^{34}S_{SO4}$ slope) is related to the net sulfate reduction rate (Böttcher et al. 1998, 1999; Aharon and Fu 2000; Antler et al. 2013; Turchyn et al.

2016). This relationship has been interpreted as a decrease in the ratio of reverse and forward fluxes during intracellular enzymatic steps with increasing sulfate reduction rate (Brunner et al. 2005; Antler et al. 2013). The net sulfate reduction rate at methane seeps is several orders of magnitude higher than that in OSR-dominated settings, resulting in the diagnostic small $\delta^{18}O_{SO4}/\delta^{34}S_{SO4}$ slope (<0.5) of SD-AOM, which is distinct from the larger $\delta^{18}O_{SO4}/\delta^{34}S_{SO4}$ slope (>0.7) in OSR-dominated settings (Aharon and Fu 2000; Feng and Robert 2011; Antler et al. 2015). Although a small $\delta^{18}O_{SO4}/\delta^{34}S_{SO4}$ slope (0.36 ± 0.06) was also observed in organic-rich sediments of mangroves (Crémière et al. 2017), the contribution of SD-AOM to the overall removal of sulfate remained uncertain, and the organic-rich environment in mangroves does not support massive carbonate precipitation (Antler and Pellerin 2018). Thus, a diagnostic small $\delta^{18}O_{SO4}/\delta^{34}S_{SO4}$ slope preserved in carbonate-associated sulfate is a robust proxy for tracing SD-AOM in the geological record (Feng et al. 2016; Tong et al. 2019).

Given the utility of this proxy, Gong et al. (2022) quantified the lowest methane flux (i.e., 200 mmol m^{-2} yr^{-1}) required to produce the diagnostic small $\delta^{18}O_{SO4}/\delta^{34}S_{SO4}$ slope of SD-AOM studying the Haima seeps of the SCS, where the contribution of OSR to overall sulfate consumption is negligible. As shown in Fig. 9.5, plotting the $\delta^{18}O_{SO4}/\delta^{34}S_{SO4}$ slope versus net sulfate reduction rates allows to distinguish between OSR– and SD-AOM-dominated settings. These observations indicated that the types of electron donors play a vital role in controlling isotope fractionation during microbial sulfate reduction in marine sediments. The $\delta^{18}O_{SO4}$ versus $\delta^{34}S_{SO4}$ patterns of porewater profiles have been widely used to explore sulfur-based reactions in marine sediments, including OSR, SD-AOM, and sulfide oxidation (Böttcher et al. 1998; Aharon and Fu 2000; Böttcher and Thamdrup 2001; Antler et al. 2014, 2015; Bertran et al. 2020). Generally, methane fluxes and the contribution of SD-AOM to overall sulfate reduction must be considered when using $\delta^{18}O_{SO4}$ versus $\delta^{34}S_{SO4}$ patterns to study the sulfur cycle.

$\delta^{18}O_{SO4}$ versus $\delta^{34}S_{SO4}$ patterns are also controlled by sulfide oxidation and the oxygen isotope composition of sulfate diffusing into the sulfate methane transition zone (SMTZ), highlighting the need for considering the pitfalls and new perspectives of this proxy (Antler and Pellerin 2018; Gong et al. 2021). First, separating SD-AOM from OSR at different depths is challenging in methane-diffusion-limited settings, where OSR in the upper sulfate reduction zone can drive $\delta^{18}O_{SO4}$ values to an apparent equilibrium value before AOM-SR can imprint its signature on the $\delta^{18}O_{SO4}$ versus $\delta^{34}S_{SO4}$ slope (Fig. 9.6). Second, the $\delta^{18}O_{SO4}$ versus $\delta^{34}S_{SO4}$ slope is affected by sulfide reoxidation in two ways: (1) sulfide reoxidation occurring in the whole sulfate reduction zone can increase the $\delta^{18}O_{SO4}$ versus $\delta^{34}S_{SO4}$ slope; (2) quantitative reoxidation of sulfide in the subsurface can alter the initial sulfur and oxygen isotope composition of porewater sulfate. With a higher or lower initial $\delta^{18}O_{SO4}$ value, $\delta^{18}O_{SO4}$ can reach the apparent equilibrium value faster or slower, respectively, consequently resulting in a greater or smaller $\delta^{18}O_{SO4}$ versus $\delta^{34}S_{SO4}$ slope

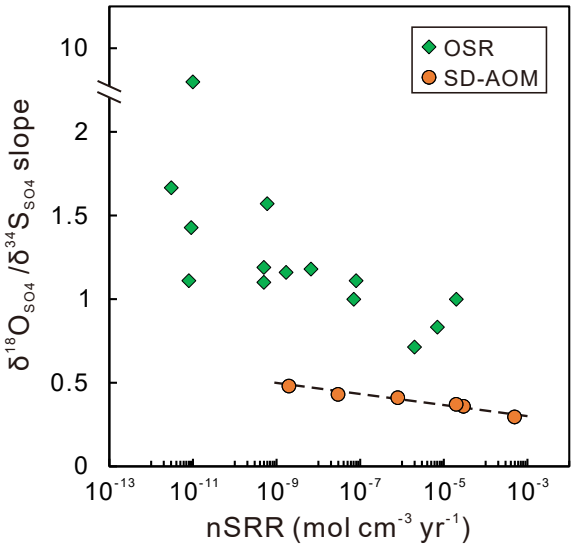

Fig. 9.5 Slope of $\delta^{18}O_{SO4}$ versus $\delta^{34}S_{SO4}$ in the apparent linear phase versus the average net sulfate reduction rate (nSRR; modified after Gong et al. 2021). *Note* OSR and SD-AOM denote organoclastic sulfate reduction and sulfate-driven anaerobic oxidation of methane, respectively. Reprinted from Chemical Geology, 581, Gong et al. (2021) Deciphering the sulfur and oxygen isotope patterns of sulfate-driven anaerobic oxidation of methane, 120394, Copyright (2021), with permission from Elsevier

(Turchyn et al. 2010), respectively. The occurrence and extent of sulfur reoxidation depend on the relative sulfate reduction rate and oxidant replenishment, which vary with the sedimentary environment (Gong et al. 2021). Third, the $\delta^{18}O_{SO4}$ versuss $\delta^{34}S_{SO4}$ slope also depends on the oxygen isotope composition of marine sulfate (Turchyn et al. 2010; Feng et al. 2016; Antler et al. 2017), which has likely changed during Earth history (Claypool et al. 1980). Finally, $\delta^{18}O_{SO4}$ values associated with SD-AOM are diagnostically higher than typical apparent equilibrium $\delta^{18}O_{SO4}$ values in OSR-dominated settings and can serve as a new proxy for the SD-AOM activity (Gong et al. 2021) because the increase in $\delta^{18}O_{SO4}$ is not limited in the course of microbial sulfate reduction with kinetically dominated oxygen isotope fractionation (Turchyn et al. 2010). With the above factors considered, the combined use of $\delta^{18}O_{SO4}$ versus $\delta^{34}S_{SO4}$ is a promising proxy to trace the sulfur cycle in modern and ancient marine sediments.

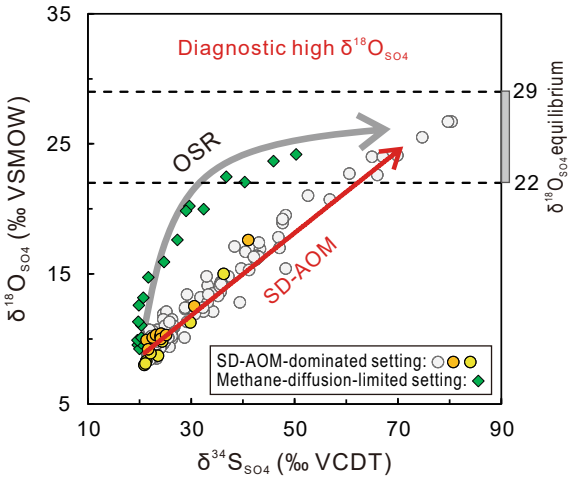

Fig. 9.6 Schematic plots of $\delta^{18}O_{SO4}$ and $\delta^{34}S_{SO4}$ for porewater sulfate at methane seeps. The red arrow denotes a linear correlation between $\delta^{18}O_{SO4}$ and $\delta^{34}S_{SO4}$ with a small slope in an SD-AOM-dominated setting (barite data are marked by gray cycles with data from Feng and Roberts (2011); the colored circles denote porewater data obtained from Gong et al. (2021)). The green diamond is the porewater sulfate profile of core W19-15, representing a methane-diffusion-limited setting (Hu et al. 2020). The gray arrow indicates an increase in $\delta^{18}O_{SO4}$ and $\delta^{34}S_{SO4}$ values at the onset of the curve in OSR-dominated settings, with $\delta^{18}O_{SO4}$ reaching apparent equilibrium values (22–29‰; Wortmann et al. 2007; Turchyn et al. 2016). *Note* OSR and SD-AOM denote organoclastic sulfate reduction and sulfate-driven anaerobic oxidation of methane, respectively

9.3 Biogeochemical Processes Archived in Authigenic Sulfides

9.3.1 High $\delta^{34}S$ Values Indicative of Enhanced Pyrite Formation

^{34}S-enriched pyrite preserved in continental-margin sediments has been used to trace the paleo-SMTZ (Jørgensen et al. 2004; Peketi et al. 2012, 2015; Lin et al. 2016a, b, 2017; Wang et al. 2018). During microbial sulfate reduction, ^{32}S is preferentially distilled into reduced products, resulting in the formation of ^{34}S-depleted pyrite. Distinct from pyrite derived from OSR, SD-AOM-derived pyrite is generally characterized by a higher $\delta^{34}S_{py}$ values due to (1) the smaller magnitude of sulfur isotope fractionation for SD-AOM (e.g., <40‰) than that for OSR and (2) higher rates of SD-AOM than OSR rates, causing accumulation of dissolved sulfide to high concentrations due to relatively closed system conditions with little sulfate replenishment and high sulfate consumption rates (Aharon and Fu 2000; Deusner et al. 2014; Gong et al. 2018a). However, ^{34}S-enriched pyrite may not develop in settings with a major contribution of OSR to pyrite formation, low iron availability, and intense sulfide

reoxidation reactions (Borowski et al. 2013; Lin et al. 2016a, b; Formolo and Lyons 2013; Pierre 2017; Feng et al. 2018).

Recent work on the sulfur isotopic signature of SD-AOM-derived pyrite in sediments and carbonates retrieved from seeps of the SCS resulted in a better understanding of pyritization in the SMTZ and the control of dynamic methane fluxes on $\delta^{34}S_{py}$ values (Pu et al. 2007; Li et al. 2016; Lin et al. 2016a, b, 2017; Hu et al. 2017, 2020; Gong et al. 2018a, 2022). The typical $\delta^{34}S$ value of OSR-derived pyrite in the continental slope of the SCS ranges from −50‰ to −20‰ (Hu et al. 2015, 2018; Lin et al. 2017; Wang et al. 2018), whereas the $\delta^{34}S_{py}$ of SD-AOM-derived pyrite is typically higher than −20‰ due to the low sulfur isotope fractionation during SD-AOM (<40‰; Aharon and Fu 2000; Deusner et al. 2014; Gong et al. 2021). Combined with the high ratios of total sulfur to total organic carbon, the widely observed high $\delta^{34}S_{py}$ values in the SMTZ indicate extensive methane seepage activity along the continental margin of the SCS (Feng et al. 2018). The extremely high nanoSIMS $\delta^{34}S$ values of SD-AOM-derived pyrite reported for the SCS reach 130.3‰, representing the heaviest stable sulfur isotope composition of pyrite ever reported to our the best of our knowledge in a marine sedimentary environment and reflecting the great variability of $\delta^{34}S$ values of SD-AOM-derived pyrite (Lin et al. 2016b; Guo et al. 2022).

Figure 9.7a provides a schematic diagram of the environmental controls on the $\delta^{34}S$ value of pyrite under high methane flux with the SMTZ close to the seafloor, dissolved sulfide accumulating to high concentrations, and the $\delta^{34}S$ value of porewater sulfide generally increasing with depth from −20‰ to approximately 21‰. Under such conditions, pyrite is only moderately ^{34}S-enriched as supported by the typical $\delta^{34}S$ value of pyrite enclosed in methane-derived authigenic carbonates (Feng et al. 2016; Gong et al. 2018b; Crémière et al. 2020; Sun et al. 2020a). Figure 9.7b depicts a methane-diffusion-limited setting with a relatively deep SMTZ, where OSR causes porewater sulfate diffusion into the SMTZ resulting in high $\delta^{34}S$ values. Under such conditions, isotopically super-heavy pyrite can form in the SMTZ. Overall, the $\delta^{34}S$ value of SD-AOM-derived pyrite can be used to trace the relative methane flux and the dynamics of methane seepage (Gong et al. 2018a, 2022). However, potential admixture of early OSR-derived pyrite during the extraction of chromium-reducible sulfides can mask the $\delta^{34}S_{py}$ signatures of SD-AOM. Fortunately, such signatures have been detected for hand-picked pyrite (Lin et al. 2016a, b), via mass-balance calculations (Hu et al. 2020; Gong et al. 2022), and through petrographic study of authigenic pyrite combined with nanoSIMS analysis of stable sulfur isotopes (Lin et al. 2016a, b).

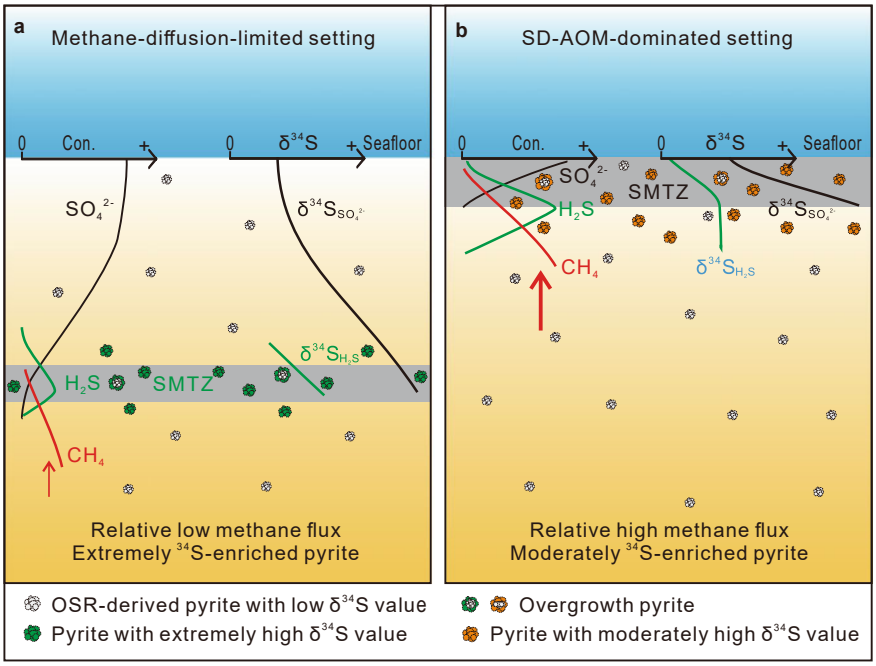

Fig. 9.7 Schematic diagram of the variable sulfur isotope composition of pyrite at methane seeps. **a** Under a relatively low methane flux with a deep SMTZ (i.e., a methane-diffusion-limited setting), the OSR progress at shallow depth causes ^{34}S-enriched sulfate to diffuse into the SMTZ, leading to a high δ^{34}S value of SD-AOM-derived pyrite exceeding the value of seawater sulfate. **b** Under a relatively high methane flux with the whole sulfate reduction zone dominated by SD-AOM (i.e., SD-AOM-dominated setting), SD-AOM-derived pyrite is moderately ^{34}S-enriched, with δ^{34}S values generally ranging from −20‰ to ca. 21‰. *Note* OSR, SD-AOM and SMTZ denote organoclastic sulfate reduction, sulfate-driven anaerobic oxidation of methane, and sulfate methane transition zone, respectively

9.3.2 Multiple Sulfur Isotope Fingerprints of SD-AOM

Recently, multiple sulfur isotopes have been applied to identify SD-AOM and to constrain the sulfur cycle in methane-bearing settings; such approach became necessary because of the common overlap of $\delta^{34}S_{py}$ values between OSR- and SD-AOM-derived pyrite (Lin et al. 2017, 2018; Gong et al. 2018b, 2022; Crémière et al. 2020; Liu et al. 2020, 2022a). The multiple sulfur isotope proxy relies on the fact that sulfur-based reactions experience varying dependencies on the expression of mass that can yield small deviations (Eq. 9.1) from thermodynamic equilibrium predictions at 0.515 (Farquhar et al. 2003; Johnston 2011). The small deviation of δ^{33}S from the mass-dependent fractionation law can be expressed with the following capital delta notation (Eq. 9.3):

$$^{33}\theta = \frac{ln^{33}\alpha}{ln^{34}\alpha} \tag{9.1}$$

$$\delta^{3i} = (^{3i}R/^{3i}R_{VCDT} - 1) * 1000, i = 3, 4 \tag{9.2}$$

$$\Delta^{33}S = \delta^{33}S - 1000 * ((\delta^{34}S + 1)^{0.515} - 1) \tag{9.3}$$

The difference in the isotope fractionation factor ($^{34}\alpha$ and $^{33}\theta$) among sulfur-based reactions can yield different relationships among multiple sulfur isotope compositions (^{32}S, ^{33}S, and ^{34}S) of sulfur-bearing compounds, which are expressed by $\Delta^{33}S$-$\delta^{34}S$ patterns. Combined $\Delta^{33}S$ and $\delta^{34}S$ analysis provides further constraints on the processes that contribute to sulfur cycling and help differentiating among various sulfur-based reactions including OSR, SD-AOM, sulfide oxidation, and sulfur disproportionation (Farquhar et al. 2003; Johnston et al. 2005; Lin et al. 2017; Gong et al. 2018b, 2022; Liu et al. 2022a). Below, we conclude that the diagnostic multiple sulfur isotope signatures of SD-AOM expressed in sulfur-bearing minerals are controlled by the low sulfur isotope fractionation during SD-AOM and the mass-transport effect on the isotope composition of dissolved sulfate and dissolved sulfide.

For a given porewater profile, the $\Delta^{33}S_{SO4} - \delta^{34}S_{SO4}$ pattern is mainly determined by the isotope fractionation of net sulfate reduction, with lower $1000\ln^{34}\alpha$ and higher $^{33}\theta$ values leading to a larger slope of $\Delta^{33}S_{SO4} - \delta^{34}S_{SO4}$ (Gong et al. 2018b; Masterson et al. 2018). In OSR-dominated settings (Fig. 9.8a), the positive $\Delta^{33}S_{SO4}$ - $\delta^{34}S_{SO4}$ pattern can be attributed to the low $1000\ln^{34}\alpha$ value and high $^{33}\theta$ value close to the equilibrium values at −70‰ and 0.515, respectively (Gong et al. 2018b, 2022; Masterson et al. 2018, 2022; Liu et al. 2022a). In SD-AOM-dominated settings (Fig. 9.8b), the relatively high $1000\ln^{34}\alpha$ (> −40‰) and $^{33}\theta$ values (<0.5125) yield negative $\Delta^{33}S_{SO4} - \delta^{34}S_{SO4}$ correlations according to the simplified reaction-transport model (Gong et al. 2018b). In methane-diffusion-limited settings (Fig. 9.8c), the pore-water sulfate profile attains a positive $\Delta^{33}S_{SO4}$ - $\delta^{34}S_{SO4}$ correlation in the upper sulfate reduction zone dominated by OSR, which switches to a negative $\Delta^{33}S_{SO4} - \delta^{34}S_{SO4}$ correlation in the SMTZ. Overall, diagnostic negative $\Delta^{33}S_{SO4} - \delta^{34}S_{SO4}$ patterns of porewater sulfate profile in the SMTZ are distinguishable from the positive trajectory in OSR-dominated settings, highlighting that multiple sulfur isotope fractionation during microbial sulfate reduction is affected by the electron donor type, which facilitates the use of this proxy to identify SD-AOM (Gong et al. 2018b, 2022; Crémière et al. 2020; Liu et al. 2022a).

Under high methane fluxes, such as methane seeps with advective transport, the diagnostic negative $\Delta^{33}S_{SO4} - \delta^{34}S_{SO4}$ correlation of SD-AOM can be preserved in barite and carbonate-associated sulfate, thus serving as a useful proxy for SD-AOM in the rock record (Gong et al. 2018b; Crémière et al. 2020). Sulfate, for example recovered from carbonate rock in the form of carbonate-associated sulfate, does not represent a single steady-state pore-water profile but rather different stages of pore water evolution indicating various successive mixtures of porewater sulfate at

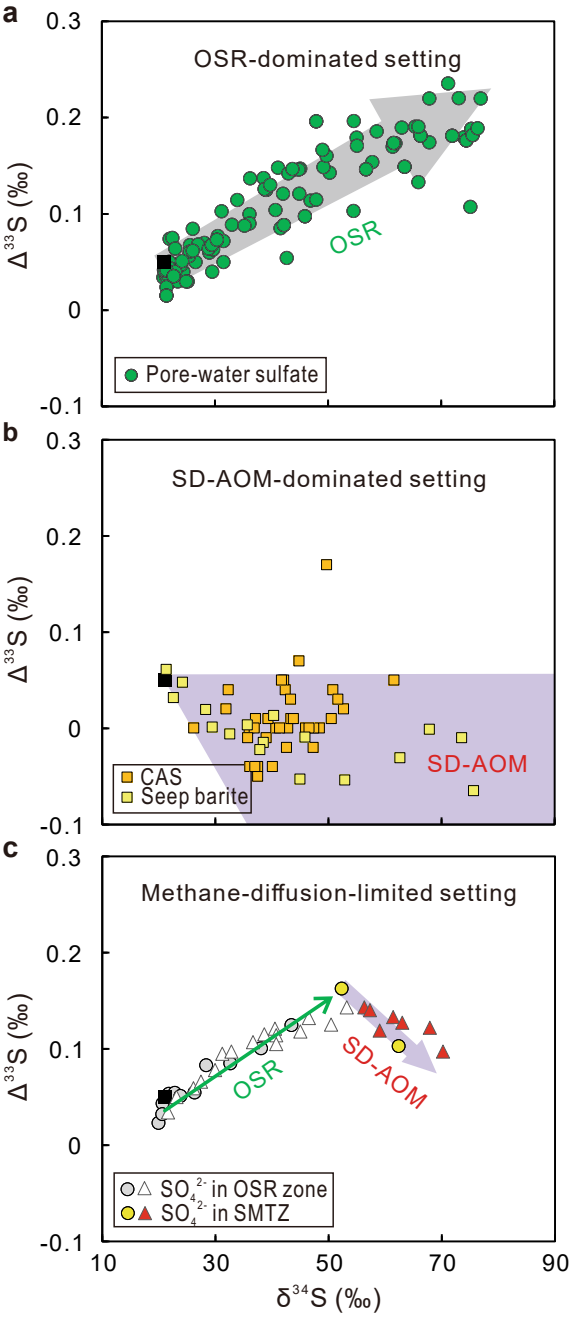

Fig. 9.8 Schematic plots of $\Delta^{33}S$ and $\delta^{34}S$ for porewater sulfate in different marine settings. **a** OSR-dominated setting (data from Strauss et al. (2012); Pellerin et al. (2015); Lin et al. (2017); Masterson et al. (2018); Gong et al. (2022); Liu et al. (2022a)); **b** SD-AOM-dominated setting, such as methane seeps (data from Gong et al. (2018b); Crémière et al. (2020)). **c** Methane-diffusion-limited setting (data retrieved from Gong et al. (2022); Liu et al. (2022a)). The black square denotes the seawater sulfate value of Tostevin et al. (2014). *Note* OSR and SD-AOM denote organoclastic sulfate reduction and sulfate-driven anaerobic oxidation of methane, respectively. Reprinted from Chemical Geology, 581, Gong et al. Reprinted from Earth and Planetary Science Letters, 597, Gong et al. (2022) Multiple sulfur isotope systematics of pyrite for tracing sulfate-driven anaerobic oxidation of methane, 117827, Copyright (2022), with permission from Elsevier

different depths. Consequently, negative $\Delta^{33}S_{SO4} - \delta^{34}S_{SO4}$ correlations cannot be expected to be necessarily archived in barite and carbonate-associated sulfate even if SD-AOM was a prominent process. The mixture of two endmembers with different $\delta^{34}S$ values can lead to a lower $\Delta^{33}S$ value than that of at least one of the endmembers (Ono et al. 2006; Johnston 2011). Thus, $\Delta^{33}S_{SO4}$ values more negative than that of seawater coupled with high $\delta^{34}S_{SO4}$ values preserved in the rock record constitute a diagnostic signature of SD-AOM at methane seeps, sites typified by advective transport of methane (Gong et al. 2022). Globally, methane-diffusion-limited environments are more widely distributed along continental margins than methane seeps (Egger et al. 2018; Hu et al. 2022). Due to the absence of methane-derived authigenic carbonates, however, the diagnostic multiple sulfur isotope signature of porewater sulfate in a methane-diffusion-limited setting can hardly be preserved in carbonate rock or barite.

Case studies on methane-bearing environments of the SCS indicated that multiple sulfur isotope compositions of pyrite can be used for tracing SD-AOM in methane diffusion-limited settings (Lin et al. 2017; Gong et al. 2022). The instantaneously produced sulfide inherits the same $\Delta^{33}S_{SO4} - \delta^{34}S_{SO4}$ trajectory of porewater sulfate, i.e., positive and negative correlations in OSR– and SD–AOM-dominated settings, respectively. However, the porewater sulfide accumulating in the course of sulfate reduction shows similar $\Delta^{33}S - \delta^{34}S$ patterns and approaches the sulfur isotopic composition of seawater sulfate in both organic compound-rich settings (Liu et al. 2022a) and, thus, is expected to occur at methane seeps (Gong et al. 2022). This phenomenon can be explained by the independent diffusion of ^{32}S, ^{33}S, and ^{34}S in sulfide in a setting where dissolved sulfide accumulates to high concentrations (e.g., >1 mmol/l; Jørgensen et al. 2004; Liu et al. 2022a; Masterson et al. 2022). Therefore, multiple sulfur isotopes of pyrite cannot trace SD-AOM activity at methane seeps and in organic-rich settings, as evidenced by the overlap of the $\Delta^{33}S_{py} - \delta^{34}S_{py}$ areas of successively formed, composite pyrite derived from SD-AOM and OSR (Fig. 9.9b).

However, the diffusion effect of porewater sulfide is limited in organic-poor deeper settings such as the continental slope sediment of the SCS, where low sulfate reduction rates led to an excess of buried reactive iron and a low concentration of dissolved sulfide. Under this circumstance, the diffusion effect on the isotope composition of porewater sulfide and the contribution of OSR-derived sulfide to the sulfide pool in the SMTZ is limited. Consequently, the increased $\Delta^{33}S$ and $\delta^{34}S$ signatures of porewater sulfate diffusing into the SMTZ can be archived in pyrite, with the $\Delta^{33}S$ value of the produced sulfide reaching as high as 0.3‰ in the upper SMTZ. Furthermore, the $\Delta^{33}S$ values of instantaneously produced sulfide within the SMTZ decrease with increasing $\delta^{34}S$ value, thus leading to a pronounced negative $\Delta^{33}S_{py}$ value falling out of the $\Delta^{33}S_{py} - \delta^{34}S_{py}$ area of the OSR. Therefore, the diagnostic larger $\Delta^{33}S - \delta^{34}S$ field of pyrite relative to OSR-derived pyrite allows tracing of SD-AOM in continental slope settings (Fig. 9.9c).

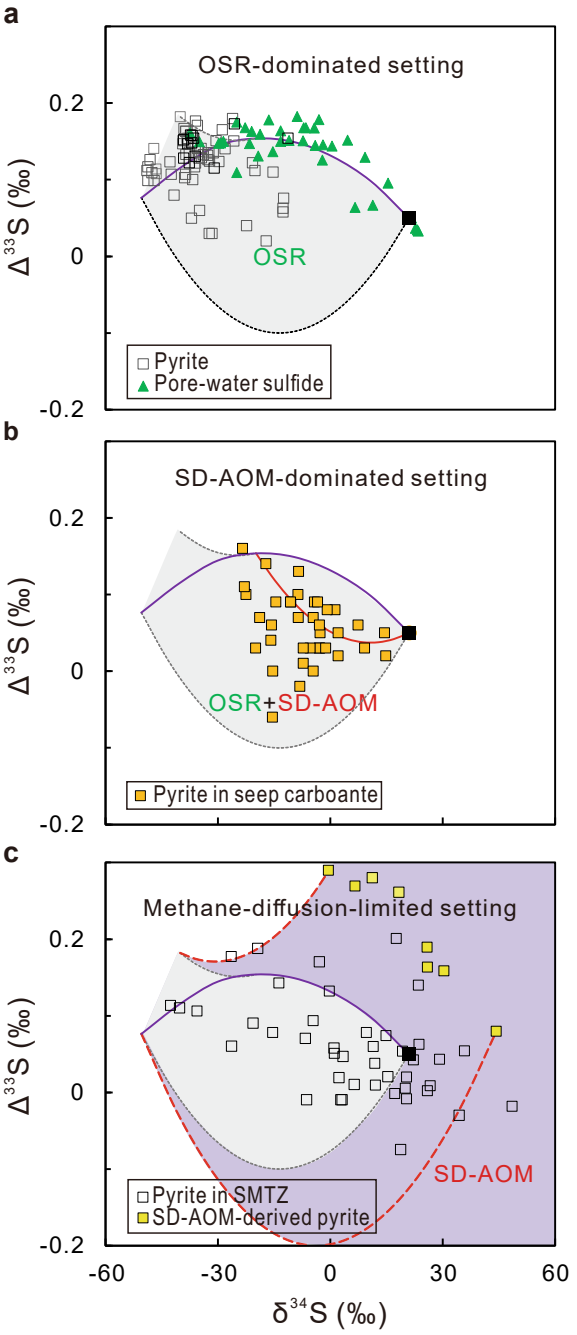

Fig. 9.9 Schematic plots of $\Delta^{33}S$ and $\delta^{34}S$ for porewater sulfide and authigenic pyrite in different marine settings: **a** OSR-dominated setting (data from Johnston et al. (2008); Strauss et al. (2012); Lin et al. (2017); Gong et al. (2022); Liu et al. (2022a)); **b** SD-AOM-dominated setting, such as methane seeps (data obtained from Crémière et al. (2020)). **c** Methane-diffusion-limited setting (data from Lin et al. (2017); Gong et al. (2022); Liu et al. (2022a)). The black square indicates the seawater sulfate value of Tostevin et al. (2014). The gray shaded area denotes the largest $\Delta^{33}S$–$\delta^{34}S$ field of pyrite in the OSR-dominated setting, and the purple area denotes the $\Delta^{33}S$–$\delta^{34}S$ field of SD-AOM-derived pyrite (modified from Gong et al. (2022)). *Note* OSR and SD-AOM denote organoclastic sulfate reduction and sulfate-driven anaerobic oxidation of methane, respectively. Reprinted from Earth and Planetary Science Letters, 597, Gong et al. (2022) Multiple sulfur isotope systematics of pyrite for tracing sulfate-driven anaerobic oxidation of methane, 117827, Copyright (2022), with permission from Elsevier

9.4 Summary and Future Studies

Widespread methane seepage along the continental margins of the South China Sea provides the opportunity to study methane-related biogeochemical processes and their fingerprints in the sedimentary record, allowing to trace the occurrence and strength of methane seepage and its effect on local to global marine environments through geologic time. Previous work on authigenic minerals formed at methane seeps in the SCS mainly aimed to reconstruct the origin of seep fluids and seepage dynamics and to establish proxies for tracing past SD-AOM activity. One of the outstanding achievements in this endeavor is our improved understanding of the sulfur isotope systematics of SD-AOM, owed to in situ nanoSIMS analysis and multiple sulfur isotopes. The latter analytical approaches allow confident identification of the origin of early diagenetic pyrite, the most common mineral at marine seeps. With respect to the South China Sea–now representing one of the best studied seepage provinces–further research targeting quantification of sulfur cycling will probably provide fundamental knowledge of the effect of SD-AOM on ocean margin sediments. Other biogeochemical processes taking place in association with SD-AOM, such as processes involving nitrogen, need to be further investigated to fully unravel the interaction between carbon, sulfur, and nitrogen cycling at marine methane seeps.

Acknowledgements Funding was provided by the NSF of China (Grants: 42225603, 41906046, and 42176056). Yu Hu and Min Luo are thanked for their constructive comments, which have greatly improved the quality of the chapter.

References

Aharon P, Fu BS (2000) Microbial sulfate reduction rates and sulfur and oxygen isotope fractionations at oil and gas seeps in deepwater Gulf of Mexico. Geochim Cosmochim Acta 64(2):233–246

Anderson TF, Arthur MA (1983) Stable isotopes of oxygen and carbon and their application to sedimentologic and paleoenvironmental problems. In: Stable Isotopes in Sedimentary Geology. SEPM (Society for Sedimentary Geology): Dallas TX USA pp 1–151

Antler G, Pellerin A (2018) A critical look at the combined use of sulfur and oxygen isotopes to study microbial metabolisms in methane-rich environments. Front Microbiol 9:519

Antler G, Turchyn AV, Rennie V et al (2013) Coupled sulfur and oxygen isotope insight into bacterial sulfate reduction in the natural environment. Geochim Cosmochim Acta 118:98–117

Antler G, Turchyn AV, Herut B et al (2014) Sulfur and oxygen isotope tracing of sulfate driven anaerobic methane oxidation in estuarine sediments. Estuar Coast Shelf Sci 142:4–11

Antler G, Turchyn AV, Herut B et al (2015) A unique isotopic fingerprint of sulfate-driven anaerobic oxidation of methane. Geology 43(7):619–622

Antler G, Turchyn AV, Ono S et al (2017) Combined ^{34}S, ^{33}S and ^{18}O isotope fractionations record different intracellular steps of microbial sulfate reduction. Geochim Cosmochim Acta 203:364–380

Bertran E, Waldeck A, Wing BA et al (2020) Oxygen isotope effects during microbial sulfate reduction: applications to sediment cell abundances. ISME J 14(6):1508–1519

Boetius A, Ravenschlag K, Schubert CJ et al (2000) A marine microbial consortium apparently mediating anaerobic oxidation of methane. Nature 407(6804):623–626

Bohrmann G, Greinert J, Suess E et al (1998) Authigenic carbonates from the Cascadia subduction zone and their relation to gas hydrate stability. Geology 26(7):647–650

Borowski WS, Rodriguez NM, Paull CK et al (2013) Are ^{34}S-enriched authigenic sulfide minerals a proxy for elevated methane flux and gas hydrates in the geologic record? Mar Pet Geol 43:381–395

Bristow TF, Grotzinger JP (2013) Sulfate availability and the geological record of cold-seep deposits. Geology 41(7):811–814

Brunner B, Bernasconi SM, Kleikemper J et al (2005) A model for oxygen and sulfur isotope fractionation in sulfate during bacterial sulfate reduction processes. Geochim Cosmochim Acta 69(20):4773–4785

Burton EA (1993) Controls on marine carbonate cement mineralogy-review and reassessment. Chem Geol 105(1–3):163–179

Böttcher ME, Thamdrup B (2001) Anaerobic sulfide oxidation and stable isotope fractionation associated with bacterial sulfur disproportionation in the presence of MnO_2. Geochim Cosmochim Acta 65(10):1573–1581

Böttcher ME, Brumsack HJ, de Lange GJ (1998) Sulfate reduction and related stable isotope (^{34}S, ^{18}O) variations in interstitial waters from the eastern Mediterranean. In: Robertson AHF, Emeis KC, Richter C et al (Eds) Proc. ODP, Sci. Results, Vol. 16. Ocean Drilling Program, College Station, TX, pp 365–373

Böttcher ME, Bernasconi SM, Brumsack HJ (1999) Carbon, sulfur, and oxygen isotope geochemistry of interstitial waters from the western Mediterranean. In: Zahn R, Comas M C, Klaus A (Eds) Proc. ODP, Sci. Results, Vol. 161. Ocean Drilling Program, College Station, TX, pp 413–421

Campbell KA (2006) Hydrocarbon seep and hydrothermal vent paleoenvironments and paleontology: Past developments and future research directions. Paleogeogr Paleoclimatol Paleoecol 232(2–4):362–407

Chen D, Huang Y, Yuan X et al (2005) Seep carbonates and preserved methane oxidizing archaea and sulfate reducing bacteria fossils suggest recent gas venting on the seafloor in the Northeastern South China Sea. Mar Pet Geol 22(5):613–621

Chen D, Feng D, Su Z et al (2006) Pyrite crystallization in seep carbonates at gas vent and hydrate site. Mater Sci Eng C-Mater Biol Appl 26(4):602–605

Chuang PC, Dale AW, Wallmann K et al (2013) Relating sulfate and methane dynamics to geology: Accretionary prism offshore SW Taiwan. Geochem Geophy Geosy 14(7):2523–2545

Claypool GE, Holser WT, Kaplan IR et al (1980) The age curves of sulfur and oxygen isotopes in marine sulfate and their mutual interpretation. Chem Geol 28(3–4):199–260

Crémière A, Strauss H, Sebilo M et al (2017) Sulfur diagenesis under rapid accumulation of organic-rich sediments in a marine mangrove from Guadeloupe (French West Indies). Chem Geol 454:67–79

Crémière A, Pellerin A, Wing BA et al (2020) Multiple sulfur isotopes in methane seep carbonates track unsteady sulfur cycling during anaerobic methane oxidation. Earth Planet Sci Lett 532:115994

Deusner C, Holler T, Arnold GL et al (2014) Sulfur and oxygen isotope fractionation during sulfate reduction coupled to anaerobic oxidation of methane is dependent on methane concentration. Earth Planet Sci Lett 399:61–73

Egger M, Riedinger N, Mogollon JM et al (2018) Global diffusive fluxes of methane in marine sediments. Nat Geosci 11(6):421–425

Farquhar J, Johnston DT, Wing BA et al (2003) Multiple sulphur isotopic interpretations of biosynthetic pathways: implications for biological signatures in the sulphur isotope record. Geobiology 1(1):27–36

Feng D, Chen D (2015) Authigenic carbonates from an active cold seep of the northern South China Sea: New insights into fluid sources and past seepage activity. Deep-Sea Res Part II-Top Stud Oceanogr 122:74–83

Feng D, Roberts HH (2011) Geochemical characteristics of the barite deposits at cold seeps from the northern Gulf of Mexico continental slope. Earth Planet Sci Lett 309(1–2):89–99

Feng D, Peng Y, Bao H et al (2016) A carbonate-based proxy for sulfate-driven anaerobic oxidation of methane. Geology 44(12):999–1002

Feng D, Qiu J, Hu Y et al (2018) Cold seep systems in the South China Sea: An overview. J Asian Earth Sci 168:3–16

Formolo MJ, Lyons TW (2013) Sulfur biogeochemistry of cold seeps in the Green Canyon region of the Gulf of Mexico. Geochim Cosmochim Acta 119:264–285

Giggenbach WF (1992) Isotopic shifts in waters from geothermal and volcanic systems along convergent plate boundaries and their origin. Earth Planet Sci Lett 113(4):495–510

Gong S, Hu Y, Li N et al (2018a) Environmental controls on sulfur isotopic compositions of sulfide minerals in seep carbonates from the South China Sea. J Asian Earth Sci 168:96–105

Gong S, Peng Y, Bao H et al (2018b) Triple sulfur isotope relationships during sulfate-driven anaerobic oxidation of methane. Earth Planet Sci Lett 504:13–20

Gong S, Feng D, Peng Y et al (2021) Deciphering the sulfur and oxygen isotope patterns of sulfate-driven anaerobic oxidation of methane. Chem Geol 581:120394

Gong S, Izon G, Peng Y et al (2022) Multiple sulfur isotope systematics of pyrite for tracing sulfate-driven anaerobic oxidation of methane. Earth Planet Sci Lett 597:117827

Grossman EL, Ku TL (1986) Oxygen and carbon isotope fractionation in biogenic aragonite: Temperature effects. Chem Geol 59:59–74

Guan H, Feng D, Wu N et al (2016) Methane seepage intensities traced by biomarker patterns in authigenic carbonates from the South China Sea. Org Geochem 91:109–119

Guan H, Birgel D, Peckmann J et al (2018) Lipid biomarker patterns of authigenic carbonates reveal fluid composition and seepage intensity at Haima cold seeps, South China Sea. J Asian Earth Sci 168:163–172

Guo Z, Liu Y, Qin G et al (2022) Extremely variable sulfur isotopic compositions of pyrites in carbonate pipes from the northern south China sea: Implications for a non-steady microenvironment. Mar Pet Geol 146:105927

Han X, Suess E, Huang Y et al (2008) Jiulong methane reef: Microbial mediation of seep carbonates in the South China Sea. Mar Geol 249(3–4):243–256

Han X, Yang K, Huang Y (2013) Origin and nature of cold seep in northeastern Dongsha area, South China Sea: Evidence from chimney-like seep carbonates. Chin Sci Bull 58(30):3689–3697

Han X, Suess E, Liebetrau V et al (2014) Past methane release events and environmental conditions at the upper continental slope of the South China Sea: constraints by seep carbonates. Int J Earth Sci 103(7):1873–1887

Hesse R (2003) Pore water anomalies of submarine gas-hydrate zones as tool to assess hydrate abundance and distribution in the subsurface - What have we learned in the past decade? Earth-Sci Rev 61(1–2):149–179

Himmler T, Birgel D, Bayon G et al (2015) Formation of seep carbonates along the Makran convergent margin, northern Arabian Sea and a molecular and isotopic approach to constrain the carbon isotopic composition of parent methane. Chem Geol 415:102–117

Holser WT, Kaplan IR, Sakai H et al (1979) Isotope geochemistry of oxygen in the sedimentary sulfate cycle. Chem Geol 25(1–2):1–17

Hu Y, Feng D, Liang Q et al (2015) Impact of anaerobic oxidation of methane on the geochemical cycle of redox-sensitive elements at cold-seep sites of the northern South China Sea. Deep-Sea Res Part II-Top Stud Oceanogr 122:84–94

Hu Y, Chen L, Feng D et al (2017) Geochemical record of methane seepage in authigenic carbonates and surrounding host sediments: A case study from the South China Sea. J Asian Earth Sci 138:51–61

Hu Y, Luo M, Chen LY et al (2018) Methane source linked to gas hydrate system at hydrate drilling areas of the South China Sea: Porewater geochemistry and numerical model constraints. J Asian Earth Sci 168:87–95

Hu Y, Luo M, Liang Q et al (2019) Pore fluid compositions and inferred fluid flow patterns at the Haima cold seeps of the South China Sea. Mar Pet Geol 103:29–40

Hu Y, Feng D, Peckmann J et al (2020) The impact of diffusive transport of methane on pore-water and sediment geochemistry constrained by authigenic enrichments of carbon, sulfur, and trace elements: A case study from the Shenhu area of the South China Sea. Chem Geol 553:119805

Hu Y, Zhang X, Feng D et al (2022) Enhanced sulfate consumption fueled by deep-sourced methane in a hydrate-bearing area. Sci Bull 67(2):122–124

Huang H, Feng D, Guo Y et al (2022a) Organoclastic sulfate reduction in deep-buried sediments: Evidence from authigenic carbonates of the Gulf of Mexico. Chem Geol 610:121094

Huang W, Meng M, Zhang W et al (2022b) Geological, geophysical, and geochemical characteristics of deep-routed fluid seepage and its indication of gas hydrate occurrence in the Beikang Basin, Southern South China Sea. Mar Pet Geol 139:105610

Jin M, Feng D, Huang K et al (2022) Magnesium isotopes in pore water of active methane seeps of the South China Sea. Front Mar Sci 9:858860

Johnston DT (2011) Multiple sulfur isotopes and the evolution of Earth's surface sulfur cycle. Earth-Sci Rev 106(1–2):161–183

Johnston DT, Farquhar J, Wing BA et al (2005) Multiple sulfur isotope fractionations in biological systems: A case study with sulfate reducers and sulfur disproportionators. Am J Sci 305(6–8):645–660

Johnston DT, Farquhar J, Habicht KS et al (2008) Sulphur isotopes and the search for life: strategies for identifying sulphur metabolisms in the rock record and beyond. Geobiology 6(5):425–435

Jørgensen BB, Böttcher ME, Lüschen H et al (2004) Anaerobic methane oxidation and a deep H_2S sink generate isotopically heavy sulfides in Black Sea sediments. Geochim Cosmochim Acta 68(9):2095–2118

Kim ST, O'Neil JR (1997) Equilibrium and nonequilibrium oxygen isotope effects in synthetic carbonates. Geochim Cosmochim Acta 61(16):3461–3475

Li N, Feng D, Chen L et al (2016) Using sediment geochemistry to infer temporal variation of methane flux at a cold seep in the South China Sea. Mar Pet Geol 77:835–845

Liang Q, Hu Y, Feng D et al (2017) Authigenic carbonates from newly discovered active cold seeps on the northwestern slope of the South China Sea: Constraints on fluid sources, formation environments, and seepage dynamics. Deep-Sea Res Part I-Oceanogr Res Pap 124:31–41

Liang Q, Huang H, Sun Y et al (2022) New insights into the archives of redox conditions in seep carbonates from the northern South China Sea. Front Mar Sci 9:945908

Lin Q, Wang J, Fu S et al (2015) Elemental sulfur in northern South China Sea sediments and its significance. Sci China-Earth Sci 58(12):2271–2278

Lin Q, Wang J, Taladay K et al (2016a) Coupled pyrite concentration and sulfur isotopic insight into the paleo sulfate–methane transition zone (SMTZ) in the northern South China Sea. J Asian Earth Sci 115:547–556

Lin Z, Sun X, Peckmann J et al (2016b) How sulfate-driven anaerobic oxidation of methane affects the sulfur isotopic composition of pyrite: A SIMS study from the South China Sea. Chem Geol 440:26–41

Lin Z, Sun X, Lu Y et al (2017) The enrichment of heavy iron isotopes in authigenic pyrite as a possible indicator of sulfate-driven anaerobic oxidation of methane: Insights from the South China Sea. Chem Geol 449:15–29

Lin Z, Sun X, Strauss H et al (2018) Multiple sulfur isotopic evidence for the origin of elemental sulfur in an iron-dominated gas hydrate-bearing sedimentary environment. Mar Geol 403:271–284

Lin Z, Sun X, Chen K et al (2022) Effects of sulfate reduction processes on the trace element geochemistry of sedimentary pyrite in modern seep environments. Geochim Cosmochim Acta 333:75–94

Liu J, Pellerin A, Izon G et al (2020) The multiple sulphur isotope fingerprint of a sub-seafloor oxidative sulphur cycle driven by iron. Earth Planet Sci Lett 536:116165

Liu J, Pellerin A, Wang J et al (2022a) Multiple sulfur isotopes discriminate organoclastic and methane-based sulfate reduction by sub-seafloor pyrite formation. Geochim Cosmochim Acta 316:309–330

Liu Y, Wei J, Li Y et al (2022b) Seep dynamics as revealed by authigenic carbonates from the eastern Qiongdongnan Basin. South China Sea. Mar Pet Geol 142:105738

Loyd SJ, Sample J, Tripati RE et al (2016) Methane seep carbonates yield clumped isotope signatures out of equilibrium with formation temperatures. Nat Commun 7:12274

Lu Y, Sun X, Lin Z et al (2015) Cold seep status archived in authigenic carbonates: Mineralogical and isotopic evidence from Northern South China Sea. Deep-Sea Res Part II-Top Stud Oceanogr 122:95–105

Lu Y, Liu Y, Sun X et al (2017) Intensity of methane seepage reflected by relative enrichment of heavy magnesium isotopes in authigenic carbonates: A case study from the South China Sea. Deep-Sea Res Part I-Oceanogr Res Pap 129:10–21

Lu Y, Sun X, Xu H et al (2018) Formation of dolomite catalyzed by sulfate-driven anaerobic oxidation of methane: Mineralogical and geochemical evidence from the northern South China Sea. Am Miner 103(5):720–734

Lu Y, Yang X, Lin Z et al (2021) Reducing microenvironments promote incorporation of magnesium ions into authigenic carbonate forming at methane seeps: Constraints for dolomite formation. Sedimentology 68(7):2945–2964

Luff R, Wallmann K (2003) Fluid flow, methane fluxes, carbonate precipitation and biogeochemical turnover in gas hydrate-bearing sediments at Hydrate Ridge, Cascadia Margin: Numerical modeling and mass balances. Geochim Cosmochim Acta 67(18):3403–3421

Masterson A, Alperin MJ, Berelson WM et al (2018) Interpreting multiple sulfur isotope signals in modern anoxic sediments using a full diagenetic model (California-Mexico Margin: Alfonso Basin). Am J Sci 318(5):459–490

Masterson AL, Alperin MJ, Arnold GL et al (2022) Understanding the isotopic composition of sedimentary sulfide: A multiple sulfur isotope diagenetic model for Aarhus Bay. Am J Sci 322(1):1–27

Mavromatis V, Schmidt M, Botz R et al (2012) Experimental quantification of the effect of Mg on calcite-aqueous fluid oxygen isotope fractionation. Chem Geol 310:97–105

Naehr TH, Eichhubl P, Orphan VJ et al (2007) Authigenic carbonate formation at hydrocarbon seeps in continental margin sediments: A comparative study. Deep-Sea Res Part II-Top Stud Oceanogr 54(11–13):1268–1291

Olson SL, Reinhard CT, Lyons TW (2016) Limited role for methane in the mid-Proterozoic greenhouse. Proc Natl Acad Sci U S A 113(41):11447–11452

Ono S, Wing B, Johnston D et al (2006) Mass-dependent fractionation of quadruple stable sulfur isotope system as a new tracer of sulfur biogeochemical cycles. Geochim Cosmochim Acta 70(9):2238–2252

Peckmann J, Thiel V (2004) Carbon cycling at ancient methane-seeps. Chem Geol 205(3–4):443–467

Peckmann J, Reimer A, Luth U et al (2001) Methane-derived carbonates and authigenic pyrite from the northwestern Black Sea. Mar Geol 177(1–2):129–150

Peketi A, Mazumdar A, Joshi RK et al (2012) Tracing the Paleo sulfate-methane transition zones and H_2S seepage events in marine sediments: An application of C-S-Mo systematics. Geochem Geophys Geosyst 13:Q10007

Peketi A, Mazumdar A, Joao HM et al (2015) Coupled C-S-Fe geochemistry in a rapidly accumulating marine sedimentary system: Diagenetic and depositional implications. Geochem Geophys Geosyst 16(9):2865–2883

Pellerin A, Bui TH, Rough M et al (2015) Mass-dependent sulfur isotope fractionation during reoxidative sulfur cycling: A case study from Mangrove Lake, Bermuda. Geochim Cosmochim Acta 149:152–164

Peng Y, Bao H, Jiang G et al (2022) A transient peak in marine sulfate after the 635-Ma snowball Earth. Proc Natl Acad Sci U S A 119(19):e2117341119
Pierre C (2017) Origin of the authigenic gypsum and pyrite from active methane seeps of the southwest African Margin. Chem Geol 449:158–164
Pu X, Zhong S, Yu W et al (2007) Authigenic sulfide minerals and their sulfur isotopes in sediments of the northern continental slope of the South China Sea and their implications for methane flux and gas hydrate formation. Chin Sci Bull 52(3):401–407
Reeburgh WS (2007) Oceanic methane biogeochemistry. Chem Rev 107(2):486–513
Sackett WM (1978) Carbon and hydrogen isotope effects during the thermocatalytic production of hydrocarbons in laboratory simulation experiments. Geochim Cosmochim Acta 42:571–580
Smrzka D, Zwicker J, Bach W et al (2019) The behavior of trace elements in seawater, sedimentary pore water, and their incorporation into carbonate minerals: a review. Facies 65(4):1–47
Smrzka D, Feng D, Himmler T et al (2020) Trace elements in methane-seep carbonates: Potentials, limitations, and perspectives. Earth-Sci Rev 208:103263
Strauss H, Bast R, Cording A et al (2012) Sulphur diagenesis in the sediments of the Kiel Bight, SW Baltic Sea, as reflected by multiple stable sulphur isotopes. Isot Environ Healt Stud 48(1):166–179
Suess E (2018) Marine cold seeps: Background and recent advances. In: Wilkes H (ed) Hydrocarbons, Oils and Lipids: Diversity, Origin, Chemistry and Fate. Springer, Cham, pp 1–21
Sun Y, Gong S, Li N et al (2020a) A new approach to discern the hydrocarbon sources (oil vs methane) of authigenic carbonates forming at marine seeps. Mar Pet Geol 114:1–9
Sun Y, Peckmann J, Hu Y et al (2020b) Formation of tubular carbonates within the seabed of the northern South China Sea. Minerals 10(9):1–17
Thiagarajan N, Cremiere A, Blattler C et al (2020) Stable and clumped isotope characterization of authigenic carbonates in methane cold seep environments. Geochim Cosmochim Acta 279:204–219
Tong H, Feng D, Cheng H et al (2013) Authigenic carbonates from seeps on the northern continental slope of the South China Sea: New insights into fluid sources and geochronology. Mar Pet Geol 43:260–271
Tong H, Feng D, Peckmann J et al (2019) Environments favoring dolomite formation at cold seeps: A case study from the Gulf of Mexico. Chem Geol 518:9–18
Tostevin R, Turchyn AV, Farquhar J et al (2014) Multiple sulfur isotope constraints on the modern sulfur cycle. Earth Planet Sci Lett 396:14–21
Turchyn AV, Brüchert V, Lyons TW et al (2010) Kinetic oxygen isotope effects during dissimilatory sulfate reduction: A combined theoretical and experimental approach. Geochim Cosmochim Acta 74(7):2011–2024
Turchyn AV, Antler G, Byrne D et al (2016) Microbial sulfur metabolism evidenced from pore fluid isotope geochemistry at Site U1385. Glob Planet Change 141:82–90
Wacker U, Fiebig J, Todter J et al (2014) Empirical calibration of the clumped isotope paleothermometer using calcites of various origins. Geochim Cosmochim Acta 141:127–144
Wang SH, Yan W, Chen Z et al (2014) Rare earth elements in cold seep carbonates from the southwestern Dongsha area, northern South China Sea. Mar Pet Geol 57:482–493
Wang X, Li N, Feng D et al (2018) Using chemical compositions of sediments to constrain methane seepage dynamics: A case study from Haima cold seeps of the South China Sea. J Asian Earth Sci 168:137–144
Wang W, Hu YL, Muscente AD et al (2021) Revisiting Ediacaran sulfur isotope chemostratigraphy with in situ nanoSIMS analysis of sedimentary pyrite. Geology 49(6):611–616
Whiticar MJ (1999) Carbon and hydrogen isotope systematics of bacterial formation and oxidation of methane. Chem Geol 161(1–3):291–314
Wortmann UG, Chernyavsky B, Bernasconi SM et al (2007) Oxygen isotope biogeochemistry of pore water sulfate in the deep biosphere: Dominance of isotope exchange reactions with

ambient water during microbial sulfate reduction (ODP Site 1130). Geochim Cosmochim Acta 71(17):4221–4232
Yang K, Chu F, Zhu Z et al (2018) Formation of methane-derived carbonates during the last glacial period on the northern slope of the South China Sea. J Asian Earth Sci 168:173–185
Yang S, Lv Y, Liu X et al (2020) Genomic and enzymatic evidence of acetogenesis by anaerobic methanotrophic archaea. Nat Commun 11(1):3941
Zhang N, Lin M, Snyder GT et al (2019) Clumped isotope signatures of methane-derived authigenic carbonate presenting equilibrium values of their formation temperatures. Earth Planet Sci Lett 512:207–213
Zhuang C, Chen F, Cheng S et al (2016) Light carbon isotope events of foraminifera attributed to methane release from gas hydrates on the continental slope, northeastern South China Sea. Sci China-Earth Sci 59(10):1981–1995